Intermetallics 18 (2010) 399–405

Contents lists available at ScienceDirect

Intermetallics

journal homepage: www.elsevier.com/locate/intermet

Experimental study and thermodynamic assessment of ternary Mg–Zn–Ce phase relations focused on Mg-rich alloys

Chen-nan Chiu [a,b], Joachim Gröbner [a], Artem Kozlov [a], Rainer Schmid-Fetzer [a,*]

[a] Institute of Metallurgy, Clausthal University of Technology, Robert-Koch-Str. 42, D-38678 Clausthal-Zellerfeld, Germany
[b] Department of Chemical Engineering, National Tsing Hua University, 101, Sec. 2, Kuang Fu Rd., Hsin-Chu 300, Taiwan, Republic of China

ARTICLE INFO

Article history:
Received 9 July 2009
Received in revised form
24 August 2009
Accepted 25 August 2009
Available online 17 September 2009

Keywords:
A. Ternary alloy systems
B. Phase diagrams
B. Thermodynamic and thermochemical properties
D. Microstructure
E. Phase diagram, prediction

ABSTRACT

The Mg-rich part of the ternary Mg–Zn–Ce system was investigated by key samples to determine the solubilities, primary crystallization and invariant reactions. Ten alloys were prepared from pure elements and investigated by DTA/DSC and SEM/EDS. A consistent thermodynamic model of the ternary Mg–Zn–Ce system is developed for the first time by using the Calphad method. Phase diagram sections at constant 300 °C, at constant 85 at.% Mg and the liquidus projection of the Mg–Zn–Ce ternary system were calculated and compared with all available experimental data. The thermodynamic description is reasonably well supported by experimental data, especially in the Mg-rich region.

1. Introduction

Improving the mechanical properties and creep resistance of magnesium alloys at elevated temperatures may significantly extend the application limits of such lightweight alloys. In that context Mg–Zn alloys are considered to have great potential, compared to conventional Mg–Al alloys, as reviewed by Bamberger [1]. In order to attain improved creep resistance and strength at elevated temperatures new magnesium alloys with Zn are being developed by adding rare earth (RE) elements (Ce, Gd, and also Y) to form precipitates in these alloys by age hardening [2,3]. Cerium is a major component of misch-metal and thus is considered as the most important part in these industrially used rare earth elements. It has been reported that addition of Ce effects excellent age hardening behavior for the Mg–1.5Zn–0.2Ce (wt.%) alloy [4].

It is evident that the Mg–Zn–Ce ternary alloy system plays a prominent role among the Mg–Zn–RE systems. Precise knowledge of the phase diagram and thermodynamic properties of the Mg–Zn–Ce system are necessary for a better understanding of alloy design. It is also a key system for the construction of a thermodynamic database for multicomponent Mg-based alloys.

The thermodynamic description of the Mg–Zn–Ce ternary system has not been proposed in the literature. In order to exploit the application potential of computational thermodynamics it is essential to not only know the phase diagram but also the corresponding thermodynamic description in a consistent manner. This also leads to the most effective way to study the ternary phase diagram by a combination of selected key experimental work jointly with thermodynamic modeling using the calculation of phase diagrams (CALPHAD) method. This is the aim of the present study on the Mg–Zn–Ce alloy system.

2. Experimental data in the literature

Experimental phase diagram data in the Mg–Zn–Ce system is limited to the isothermal section at 300 °C, at 350 °C and some works in the Mg-rich corner. No complete phase diagram exists in the literature for this system. The ternary phase relations were first investigated by Korol'kov and Sal'dau [5]. The liquidus projection in the Mg-rich corner was drawn based on thermal analysis of alloys at six constant mass ratios (Ce:Zn = 1:10, 1:4.5, 1:2, 1:1, 2:1, and 5:1). A ternary eutectic was reported with liquid composition Mg–47.5wt.%Zn–2.5wt.%Ce (Mg–25.9at.%Zn–0.6at.%Ce) at 341–343 °C without providing explanation [5]. Solvus lines at 20, 200, 300, and 335 °C were also given. It is noted that in their study low purity Ce (96%) was used and the adopted Ce–Mg binary phase

* Corresponding author.
E-mail address: schmid-fetzer@tu-clausthal.de (R. Schmid-Fetzer).

0966-9795/$ – see front matter © 2009 Elsevier Ltd. All rights reserved.
doi:10.1016/j.intermet.2009.08.013

diagram differs from the currently accepted one. Therefore, the combined solubility of Ce and Zn in Mg is considered to be an estimated value. Even though, the results indicate that the solubility of Zn in (Mg) is lowered by the addition of Ce.

An isothermal section at 300 °C in the Mg–$MgZn_2$–CeMg–CeZn region was given by Mel'nik et al. [6]. They inspected this region from 150 alloys annealed for 240 h by using X-ray diffraction analysis. The result shows that most of Ce–Mg binary phases extend with a solid solubility into the ternary system. CeMg and CeZn form a continuous solid solution, and both crystallize in the same CsCl structure. Large solubilities of Zn in $CeMg_3$ and $CeMg_{12}$ at 300 °C were found, 29 at.% and 8 at.% Zn, respectively. Four ternary compounds, $CeMg_7Zn_{12}$, $Ce(Mg_{0.5-0.85}Zn_{0.5-0.15})_9$, $CeMg_3Zn_5$, and $Ce_2Mg_3Zn_3$, were discovered at 300 °C, designated as τ_1–τ_4 in the review of data up to the year 2000 by Kolitsch et al. [7]. The homogeneity range of the τ_2 phase extends from 9.1 to 45.5 at.% Zn (81.9–45.5 at.% Mg) at 9 at.% Ce at 300 °C. The τ_4 phase is homogeneous from 35 to 45 at.% Zn and from 40 to 30 at.% Mg for 25 at.% Ce at 300 °C. The crystal structure of τ_2 is reported to be Th_2Ni_{17} structure type [8], while that of τ_4 is given as $MgLi_2Ag$ or $AlMnCu_2$ structure type by Mel'nik et al. [9]. The structures of τ_1 and τ_3 are still unknown. Due to the same Th_2Ni_{17} structure type of τ_2 and $CeMg_{10.3}$, which corresponds to Ce_2Mg_{17} used in this work, it was suggested that the high temperature phase Ce_2Mg_{17} might be stabilized by the addition of zinc to form a continuous solid solution with the τ_2 ternary phase [8]. It is noted that Ce_2Mg_{17} only exists in a narrow high temperature range between 608 and 616 °C in the Ce–Mg binary system [10]. Mel'nik et al. [6] reported the τ_1 phase to be in equilibrium with Mg_7Zn_3 at 300 °C. However, the result is contradictory to the binary Mg–Zn phase diagram [11] in which the Mg_7Zn_3 phase (or $Mg_{51}Zn_{20}$) is not stable at 300 °C. The reported isotherm [6] was thus modified and re-plotted in the critical review by Kolitsch et al. [7].

Two isoplethal sections at 24 wt.% Zn and 34 wt.% Zn in the Mg-rich region were established by Drits et al. [8]. They prepared the alloys in corundum crucibles under a protective VI-2 flux {composition 38–46% $MgCl_2$, 32–40% KCl, 5–8% $BaCl_2$, 3–5% CaF_2, 1.5% MgO, and <8% ($NaCl + CaCl_2$)} in an electric furnace and examined the alloys by differential thermal analysis (DTA), microstructural, electron-microprobe, and X-ray diffraction analyses. The ternary phases τ_1 and τ_2 are also found in their study, and they labeled τ_2 as $Ce(Mg_{0.5-0.9}Zn_{0.5-0.1})_{10.1}$.

Kevorkov and Pekguleryuz [12] recently studied the Mg-rich corner of the Mg–Zn–Ce phase diagram at 350 °C by using a diffusion couple technique. They examined the solid solubilities of binary and ternary solutions by EDS and EPMA. In addition to the four ternary phases reported previously [6], two new ternary phases, $Ce_2Mg_{53}Zn_{45}$ and $Ce_6Mg_{(8-15)}Zn_{(86-79)}$, were found in their work. The decagonal quasicrystal reported in many of the Mg–Zn–RE systems was not observed in the Mg–Zn–Ce system [13]. Pavlyuk et al. reported a Heusler-type alloy with the composition $CeMgZn_2$ [14] and a cubic phase $Ce_{20}Mg_{19}Zn_{81}$ [15]. Crystallographic data and compositions of all ternary phases accepted in the present study are summarized in Table 1. True ternary phases, not originating at a binary edge, are labeled T1–T5. To avoid confusion, phase designations used by Refs. [7,12] are also given.

3. Experimental procedures

The present experimental work focuses on missing key data for thermodynamic modeling, and is also guided by such calculations with preliminary data sets as detailed later. The Mg–Zn–Ce ternary alloy samples were prepared from cerium ingot (99.9 wt.%, Santoku America Inc., Phoenix, USA), magnesium pieces (99.99 wt.%, Chempur, Karlsruhe, Germany), and zinc rods (99.98 wt.%, Harzer Zink GmbH, Goslar, Germany). Typical weight of these samples was 500 mg. In order to prevent the vaporization of Mg and Zn, the samples were not prepared by arc-melting method, since the significant loss of these metals leads to substantial change of the compositions. The weighted elements were pressed carefully to pellets which were sealed under argon atmosphere by welding in

Table 1
Solid phases existing inside the ternary Mg–Zn–Ce system.

Phase name	Phase description	Prototype	Pearson symbol/space group	Zn-solubility [at.%] at 300 °C	Reference
Ce(Mg,Zn)	$Ce(Mg,Zn)_1$	CsCl	*cP*2/*Pm*-$\bar{3}$*m*	0–100	[6]
$CeMg_2$	$Ce(Mg,Zn)_2$	$MgCu_2$	*cF*24/*Fd*-$\bar{3}$*m*	–	[6]
				0–1	This work
$CeMg_3$[a]	$Ce(Mg,Zn)_3$	BiF_3	*cF*16/*Fm*-$\bar{3}$*m*	0–29	[6]
	Phase 3 after [12]			0–48[d]	[12]
	τ_4 after [7]	$MgLi_2Ag$ or $AlMnCu_2$		0–48	This work
				35–45	[8,9]
$CeMg_{12}$[b]	$Ce(Mg,Zn)_{12}$	$ThMn_{12}$	*tI*26/*I*4/*m*	0–8	[6]
	Phase 1 after [12]			0–49[d]	[12]
	τ_2 after [7]	Th_2Ni_{17}		0–40	This work
				9.1–45.5	[8,9]
T1	$CeMg_7Zn_{12}$	hexagonal	Not known	stoichiometric	[6]
	τ_1 after [7]				
	Phase 4 after [12]				
T2	$Ce_2Mg_{53}Zn_{45}$	Not known	Not known	stoichiometric	[12]
	Phase 2 after [12]				
T3	$CeMg_3Zn_5$	Not known	Not known	stoichiometric	[6]
	τ_3 after [7]				
	Phase 5 after [12]				
T4[c]	$Ce_6Mg_{11}Zn_{83}$	Not known	Not known	79–86	[12]
	Phase 6 after [12]				
T5[c]	$CeMgZn_2$	$MnCu_2Al$	*cF*4/*Fm*-$\bar{3}$*m*	Not known	[14]
	Heusler-type alloy				

[a] The phases $CeMg_3$ and τ_4 from the assessment of Kolitsch et al. [7] were simplified to one phase, $CeMg_3$.
[b] The phases $CeMg_{12}$ and τ_2 from the assessment of Kolitsch et al. [7] were simplified to one phase, $CeMg_{12}$.
[c] The phase T4 is not modeled in this work, since no formation temperature is available for this phase. Also the phases T5, $CeMgZn_2$, and $Ce_{20}Mg_{19}Zn_{81}$ reported by Refs. [14,15] were not considered in this work, focusing on the Mg-rich region.
[d] At 350 °C.

thin-walled tantalum crucibles to avoid evaporation and oxidation. No reactions between the crucibles and the samples were observed.

After testing the tightness of the tantalum crucibles in a separate furnace, the samples 4, 6, 7, 9 and 10 were measured by DTA in a Netzsch DTA 404S apparatus. The heating/cooling rates applied were 1 K/min and 5 K/min. The overall uncertainty of DTA measurements was estimated to be less than ±4 K. The measurement of the phase transformation temperatures of the samples 1–3, 5 and 8 were carried out by differential scanning calorimetry (DSC) in a heat-flux cylindrical Calvet-type calorimetric system Multi HTC 96 (Setaram, Caluire, France). The equipment was calibrated using high purity Ag, Al, In, Mg and Pb. Helium at 2 l/h flow rate was applied as analysis chamber gas. The reference Ta-capsule was also sealed by welding, and a sapphire cylinder was used as reference material. The sapphire mass was 492.5 mg, which is a good balance for the heat capacity of the sample. The scanning program comprised cycles 100–850–100 °C at heating/cooling rates of 3 K/min and 5 K/min. The results are consistent and reproducible. The difference between heating and cooling peaks was below 4 K. The overall uncertainty of DSC measurements for temperature determination was estimated as ±3 K.

After DTA and DSC measurements, tantalum crucibles were cut to take out the samples, and the alloys were ground and polished immediately under ethanol to avoid oxidation. Then, the microstructures of the investigated alloys were observed by scanning electron microscopy (SEM), and the composition of the phases was determined by energy dispersive X-ray spectroscopy (EDS) analysis. The compositions of the ten Mg–Zn–Ce ternary alloys, which were investigated in this work are shown in Table 2. The compositions are mainly chosen, using preliminary thermodynamic calculations, to measure ternary invariant but also liquidus temperatures. Especially the formation temperatures of the ternary phases, that is the thermal stability limit of the single phase region – irrespective of the formation reaction (congruent, peritectic…) – are not reported in the literature. Additionally, the ternary solubilities of binary phases are in the focus of the present work.

Table 2
Temperatures extracted from the DTA/DSC signals obtained by thermal analysis in the Mg–Zn–Ce system.

Nr.	Sample composition [at.%]	Thermal signal [°C]		Thermodynamic calculation	
		Heating[a]	Cooling[b]	Temperature [°C]	Phase boundary/ reaction
1	Ce13–Mg85–Zn2	712 w	709 w	714	Liquidus
		620 s	611 s	617	U8
		603 w	573 w		?
2	Ce10–Mg85–Zn5	662 w	622 w	666	Liquidus
		602	597w		?
		583	582 w		?
3	Ce5–Mg85–Zn10	547	544 w		?
		520	533 w		?
4	Ce9–Mg82–Zn9	563 s	579 s		?
5	Ce42–Mg56–Zn2	730 s	727 s	730	Liquidus
		700 s	702 s		?
		658 w	594 w		?
6	Ce9–Mg45–Zn46	640 w	619 s		?
		562 s	563 s	562	Formation of T2
		541 s	538 s		?
		334 s	333 s		?
7	Ce25–Mg35–Zn40	784 s	788 s	785	Liquidus
		539 w	545 w		?
8	Ce14–Mg35–Zn51	676 s	670 s	680	P2 or E2 Scheil[c]
		558	558		?
		550	547		?
9	Ce5–Mg35–Zn60	733?	735 s	735	Formation of T1
		537 s	497 s		?
		352 w	359 w		?
		335 s	335 s		?
10	Ce11–Mg34–Zn55	679 s	689 s	680	P2 or E2 Scheil[c]
		–	642 s		?
		574 w	564 w		?
		534 w	528 w		?
		350?	334 w		?

[a] Onset for invariant reactions, peak maximum otherwise.
[b] Onset (s = strong signal, w = weak and diffuse signal).
[c] Calculated equilibrium solidification indicates P2 (680 °C) while Scheil simulation ends at E2 (681 °C).

4. Development of the Mg–Zn–Ce ternary thermodynamic description

The thermodynamic parameters of the constituent binary systems are taken from the previous works of Cacciamani et al. [10] (Ce–Mg), Wang et al. [16] (Ce–Zn), and Agarwal et al. [11] (Mg–Zn) and these thermodynamic data sets are considered to be fairly satisfactory.

The Gibbs energy function, $G_i^{0,\phi}(T) = G_i^{\phi}(T) - H_i^{\mathrm{SER}}$, for the element (i) (i = Ce, Mg, and Zn), in any phase ϕ is described by an equation of the following form,

$$G_i^{0,\phi}(T) = a + bT + cT\ln T + dT^2 + eT^3 + fT^{-1} + gT^7 + hT^{-9}, \quad (1)$$

where H_i^{SER} is the molar enthalpy of the element (i) at 298.15 K and 1 bar in its standard element reference (SER) state, which is fcc for Ce, hcp for Mg, and hcp for Zn. T is the absolute temperature. The Gibbs energy function of the element i in its SER phase, ϕ = SER, is often denoted as GHSER_i,

$$\mathrm{GHSER}_i = G_i^{0,\mathrm{SER}}(T) \quad (2)$$

The Gibbs energy functions for Ce, Mg and Zn are taken from the SGTE (Scientific Group Thermodata, Europe) compilation by Dinsdale [17].

The Gibbs energies for liquid, bcc, fcc, and hcp solution phases are described by the substitutional solution model as follows,

$$G^{\phi} = \sum_i x_i \cdot G_i^{0,\phi} + RT\sum_i x_i \ln x_i + \sum_{i,j>i} x_i \cdot x_j \cdot \sum_{\nu} L_{i,j}^{\nu,\phi} \cdot (x_i - x_j)^{\nu}, \quad (3)$$

where x_i (x_j) represents the mole fraction of element (i) (j), with (i) (j) = Ce, Mg, and Zn), R is the gas constant (R = 8.3143 J/mol K) and $L_{i,j}^{\nu,\phi}$ is the Redlich–Kister parameter representing the interaction between elements (i) and (j) [18]. This interaction parameter, $L_{i,j}^{\nu,\phi}$, may be linearly temperature dependent and is usually expressed as $L_{i,j}^{\nu,\phi} = A_{i,j}^{\nu,\phi} + B_{i,j}^{\nu,\phi} \cdot T$. In eq. (3), the first and the second terms represent the Gibbs energies for mechanical mixture of elements and ideal mixing, respectively, and the third term corresponds to the excess Gibbs energy of mixing.

As mentioned in Section 2, the binary phases CeMg and CeZn form a continuous solid solution. This phase is modeled with two sublattices and a substitutional solution on the second sublattice, $\mathrm{Ce}_1(\mathrm{Mg,Zn})_1$. Similarly, the other ternary solution phases are modeled as $\mathrm{Ce}_m(\mathrm{Mg,Zn})_n$. The Gibbs energy of the phase $\mathrm{Ce}_m(\mathrm{Mg,Zn})_n$ (per mole of atoms) is expressed in the Compound Energy Formalism (CEF) [19] by

$$\begin{aligned} G^{\mathrm{Ce}_m(\mathrm{Mg,Zn})_n} = {} & y_{\mathrm{Mg}} G^{0,\mathrm{Ce}_m\mathrm{Mg}_n}_{\mathrm{Ce:Mg}} + y_{\mathrm{Zn}} G^{0,\mathrm{Ce}_m\mathrm{Zn}_n}_{\mathrm{Ce:Zn}} \\ & + \frac{n}{m+n} RT\left(y_{\mathrm{Mg}} \ln y_{\mathrm{Mg}} + y_{\mathrm{Zn}} \ln y_{\mathrm{Zn}}\right) \\ & + y_{\mathrm{Mg}} y_{\mathrm{Zn}} \left(L^{0,\mathrm{Ce}_m(\mathrm{Mg,Zn})_n}_{\mathrm{Ce:Mg,Zn}} \right. \\ & \left. + \left(y_{\mathrm{Mg}} - y_{\mathrm{Zn}}\right) L^{1,\mathrm{Ce}_m(\mathrm{Mg,Zn})_n}_{\mathrm{Ce:Mg,Zn}} + \cdots\right) \end{aligned} \quad (4)$$

in which y_{Mg} and y_{Zn} are the site fractions of Mg and Zn on the second sublattice. $L^{0,Ce_m(Mg,Zn)_n}_{Ce:Mg,Zn}$ and $L^{1,Ce_m(Mg,Zn)_n}_{Ce:Mg,Zn}$ represents the interaction parameters, describing essentially the interaction within the sublattice, optimized in the present work. The parameters $G^{0,Ce_mMg_n}_{Ce:Mg}$ and $G^{0,Ce_mZn_n}_{Ce:Zn}$ are the Gibbs energies of the end-member phases. The end-member phases are formed when the second sublattice is occupied only by one kind of species; they can be either real or hypothetical. The Gibbs energies of CeMg and CeZn phases are real and taken directly from the binary description of the Ce–Mg [10] and Ce–Zn [16] systems. However, for the phases $CeMg_3$ and $CeMg_{12}$ with limited ternary solution ranges, the parameters $G^{0,CeMg_3}_{Ce:Zn}$ and $G^{0,CeMg_{12}}_{Ce:Zn}$ represent the metastable end-members of the solid solutions in the binary Ce–Zn system. They were given sufficiently large positive values in this work.

The ternary phases T1, T2 and T3 are modeled as stoichiometric compounds referred to the stable elements as given for the example of T1, $CeMg_7Zn_{12}$:

$$G^{T1} = 5G^{0,fcc}_{Ce}(T) + 35G^{0,hcp}_{Mg}(T) + 60G^{0,hcp}_{Zn}(T) + A + BT, \qquad (5)$$

where the parameters A and B are the enthalpy and entropy of formation of T1. The software package "Pandat" [20] is utilized for all calculations and the thermodynamic parameters for the ternary system optimized in this work are listed in Table 3.

The phase T4 reported by Ref. [12] is not modeled in this work, since no formation temperature is available for this phase. The composition lies far outside the Mg-rich area which was focused on in this work. Also the phases $CeMgZn_2$ (T5) and $Ce_{20}Mg_{19}Zn_{81}$ reported by Refs. [14,15] were not considered in the present modeling.

5. Results and discussion

5.1. Experimental results

Temperatures obtained by thermal analysis as extracted from the DTA/DSC signals are given in Table 2. Each heating/cooling signal is based on at least 2 repeated cycles of a single sample. Invariant reactions were recognized from the peak shape. The interpretations of the experimental temperatures in the last two columns are based on the thermodynamic calculation. The corresponding microstructures of slowly solidified samples are given later and discussed in detail jointly with the calculated temperatures in vertical phase diagram sections.

For the Zn-rich samples 6, 7, 9 and 10 the interpretation of DTA signals proved to be difficult. The microstructure of the alloys solidified slowly under DTA condition shows local inhomogeneities of the formed phases. During polishing a powdering of Zn-rich samples was observed. Therefore no artifact-free photos of the microstructure could be obtained.

5.2. Thermodynamic calculation of phase equilibria

Ternary parameters for the solid phases were adjusted on the one hand to meet the measured ternary invariant and liquidus temperatures. Additionally, the assessed data from literature for the homogeneity ranges of $CeMg_{12}$ and $CeMg_3$ and tie-line triangulation at 300 °C and own EDS measurements were used. The phases $CeMg_{12}$ and τ_2 from the assessment of Kolitsch et al. [7] were treated as one phase starting from the binary $CeMg_{12}$ phase and dissolving up to 40 at.% Zn. The $CeMg_3$ and τ_4 phases from that assessment [7] were also unified into a single phase starting from the binary $CeMg_3$ phase and dissolving as a line-compound up to 48 at.% Zn by substituting Mg. Although Mel'nik et al. [6] described different crystal structures for the corresponding phases, we treat them as one phase. This not only simplifies the calculation, moreover [12] did not find any two-phase field between these phases and draw the $CeMg_{12}$–τ_2-phase as one line and the $CeMg_3$–τ_4-phase with dashed triangle in their figures. The maximum Zn-solubility of $CeMg_3$ is set to the value reported by Ref. [12] (about 48 at.% Zn at 350 °C) and reproduced by the calculation as 48.1 at.% Zn (350 °C) and 47.9 at.% Zn (300 °C), respectively. The maximum Zn-solubility of $CeMg_{12}$ is set to 40 at.% Zn at 300 °C based on our own samples. At 350 °C a value of 41.5 at.% Zn is calculated, which is lower than the value reported by Ref. [12] (about 49 at.% Zn).

The liquidus temperatures of these phases from the thermal analysis (DTA/DSC) are also used to determine the thermodynamic parameters. The Zn-solubilities of $CeMg_2$ phase is measured and modeled at 1 at.% Zn, which gives an excellent fit to the measured liquidus temperature of sample #5, which is also very close to the transition reaction U1. The compositions of the ternary phase reported by Refs. [6,12] in Table 1 are confirmed for the phases T1, T2 and T3 by own EDS measurements. Their parameters are selected to reproduce both their solid state equilibria and the measured formation temperatures in Table 2: 735 °C for T1 in sample #9, 562 °C for T2 in sample #6, and 680 °C (P2) for T3 in sample #10. The invariant reaction at about 680 °C measured in samples #8 and #10 can be allocated to two different reactions, E2 and P2. These reactions are calculated closely spaced at 681 and 680 °C, respectively. Depending on the solidification path the alloy will pursue, P2 is passed under equilibrium condition but E2 under Scheil condition.

Fig. 1a shows the calculated liquidus projection of the Mg–Zn–Ce system based on the proposed thermodynamic description. It is dominated by the three binary Ce–Mg phase with large Zn-solubility: Ce(Mg,Zn), $CeMg_3$ and $CeMg_{12}$. Beside the numerous Ce–Zn phases in the Zn-rich part, larger primary fields are only visible for the (Mg) and the ternary T1 phase. The Ce_5Mg_{41} and especially Ce_2Mg_{17} phases show only small primary fields, which is also due to their small solid solubility of Zn. For the Ce-poor region of the liquidus projection a magnification of the Mg–Zn-rich edge is

Table 3
Ternary thermodynamic parameters for the Mg–Zn–Ce.

Phase name	Model	Parameters [J/(mol formula unit)]
$CeMg_{12}$	(Ce) $(Mg,Zn)_{12}$	$G^{0,CeMg_{12}}_{Ce:Zn} = -280000 + 80\cdot T + G^{0,FCC}_{Ce} + 12G^{0,HCP}_{Zn}$ $L^{0,CeMg_{12}}_{Ce:Mg,Zn} = -116000 + 50\cdot T$
$CeMg_3$	(Ce) $(Mg,Zn)_3$	$G^{0,CeMg_3}_{Ce:Zn} = -140000 + 35\cdot T + G^{0,HCP}_{Ce} + 3G^{0,HCP}_{Zn}$ $L^{0,CeMg_3}_{Ce:Mg,Zn} = -92000 + 94\cdot T$
$CeMg_2$	(Ce) $(Mg,Zn)_2$	$G^{0,CeMg_2}_{Ce:Zn} = -87000 + 27\cdot T + G^{0,HCP}_{Ce} + 2G^{0,HCP}_{Zn}$
T1	$(Ce)(Mg)_7(Zn)_{12}$	$G^{0,T1}_{Ce:Mg:Zn} = -332000 + 10\cdot T + G^{0,HCP}_{Ce} + 7G^{0,HCP}_{Mg} + 12G^{0,HCP}_{Zn}$
T2	$(Ce)_2(Mg)_{53}(Zn)_{45}$	$G^{0,T2}_{Ce:Mg:Zn} = -1100000 + 50\cdot T + 2G^{0,HCP}_{Ce} + 53G^{0,HCP}_{Mg} + 45G^{0,HCP}_{Zn}$
T3	$(Ce)(Mg)_3(Zn)_5$	$G^{0,T3}_{Ce:Mg:Zn} = -240000 + 67\cdot T + G^{0,HCP}_{Ce} + 3G^{0,HCP}_{Mg} + 5G^{0,HCP}_{Zn}$

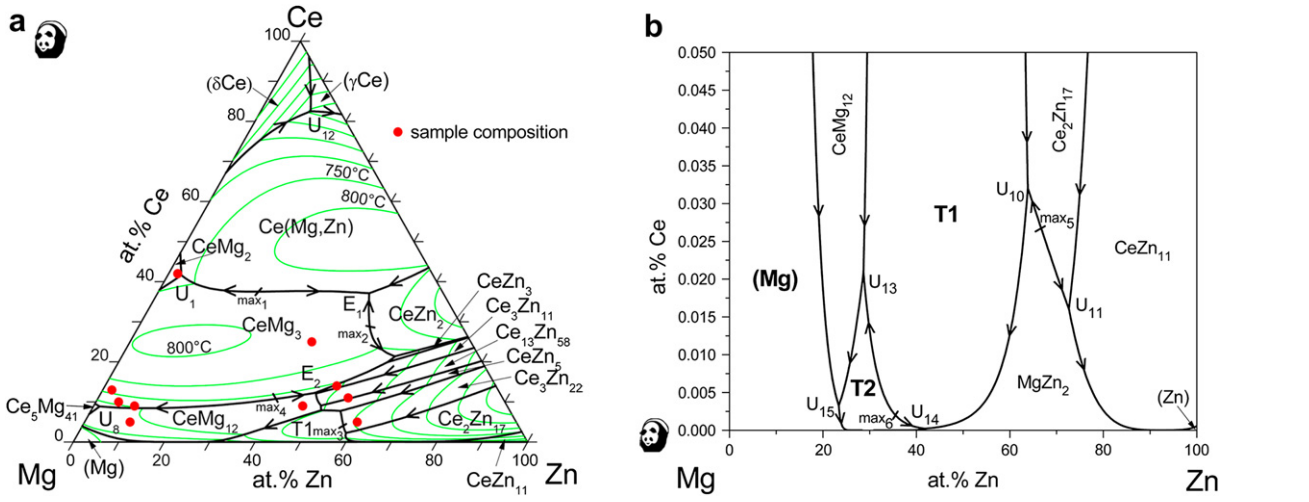

Fig. 1. (a) Calculated liquidus projection of the Mg–Zn–Ce system; superimposed are the present sample compositions. (b) Magnified Mg–Zn-rich edge of (a).

shown in Fig. 1b. The small primary fields of T2 and $MgZn_2$ and the locations of the invariant reactions U10, U11, U13, U14 and U15 can be seen. The calculated invariant reactions are given in Table 4. They also comprise six more invariant reactions below U15 in the temperature range 415.8–340.99 °C. These six reactions cannot be seen in Fig. 1b since their calculated liquid composition is even below 10^{-5} at.% Ce. That is, they are entirely degenerate to the corresponding six invariant reactions of the binary Mg–Zn system.

Table 4
Calculated invariant reactions compared with measured temperatures.

Type	Reaction	Temperature [°C]	
		Calculated [This work]	Experimental [This work]
max1	$L \rightarrow CeMg_3 + Ce(Mg,Zn)$	770.3	
max2	$L \rightarrow CeMg_3 + CeZn_2$	766.2	
E1	$L \rightarrow CeMg_3 + CeZn_2 + Ce(Mg,Zn)$	739.1	
max3	$L + Ce_3Zn_{22} \rightarrow T1$	735.2	735
U1	$L + CeMg_3 \rightarrow Ce(Mg,Zn) + CeMg_2$	729.7	
U2	$L + CeZn_2 \rightarrow CeMg_3 + CeZn_3$	726.7	
U3	$L + Ce_3Zn_{22} \rightarrow T1 + Ce_2Zn_{17}$	724.9	
U4	$L + CeZn_3 \rightarrow Ce_3Zn_{11} + CeMg_3$	720.6	
U5	$L + Ce_3Zn_{22} \rightarrow T1 + CeZn_5$	715.3	
P1	$L + T1 + CeZn_5 \rightarrow CeMg_{12}$	697.1	
U6	$L + CeZn_5 \rightarrow CeMg_{12} + Ce_{13}Zn_{58}$	694.9	
max4	$L \rightarrow CeMg_{12} + CeMg_3$	682.6	
U7	$L + Ce_{13}Zn_{58} \rightarrow CeMg_{12} + Ce_3Zn_{11}$	681.9	
E2	$L \rightarrow CeMg_{12} + Ce_3Zn_{11} + CeMg_3$	681.0	678[a]
P2[b]	$Ce_{13}Zn_{58} + CeMg_{12} + Ce_3Zn_{11} \rightarrow T3$	680.2	678[a]
U8	$L + CeMg_3 \rightarrow CeMg_{12} + Ce_5Mg_{41}$	616.7	615
U9	$L + Ce_5Mg_{41} \rightarrow CeMg_{12} + Ce_2Mg_{17}$	613.2	
max5	$L \rightarrow MgZn_2 + Ce_2Zn_{17}$	589.8	
U10	$L + Ce_2Zn_{17} \rightarrow T1 + MgZn_2$	588.1	
U11	$L + Ce_2Zn_{17} \rightarrow MgZn_2 + CeZn_{11}$	581.3	
U12	$L + \delta Ce \rightarrow Ce(Mg,Zn) + \gamma Ce$	542.3	
max6	$L + T1 \rightarrow T2$	489.5	
U13	$L + T1 \rightarrow CeMg_{12} + T2$	480.4	
U14	$L + T1 \rightarrow T2 + MgZn_2$	479.1	
U15	$L + CeMg_{12} \rightarrow (Mg) + T2$	420.3	
U16	$L + MgZn_2 \rightarrow T2 + Mg_2Zn_3$	415.8	
U17	$L + MgZn_2 \rightarrow Mg_2Zn_{11} + CeZn_{11}$	381.2	
E3	$L \rightarrow Mg_2Zn_{11} + (Zn) + CeZn_{11}$	367.2	
U18	$L + Mg_2Zn_3 \rightarrow MgZn + T2$	347.0	
U19	$L + (Mg) \rightarrow Mg_7Zn_3 + T2$	341.02	
E4	$L \rightarrow MgZn + Mg_7Zn_3 + T2$	340.99	

[a] Strong thermal signals of samples #8 and #10 are evaluated at 678 °C and could be assigned to P2 or E2, see Table TX2.

[b] P2 at 680.2 °C is the only solid state reaction in this list; compound T3 is formed in this peritectoid-type invariant reaction.

Two of them, U17 and E3, are on the Zn-rich side and equilibrate with $CeZn_{11}$, while the other four, U16, U18, U19 and E4, are on the Mg-rich side and equilibrate with T2. There are only two invariant reactions involving liquid and the (Mg) solid solution phase, U15 and U19, followed very closely by the deepest eutectic, E4.

The calculated isothermal section at 300 °C is given in Fig. 2. Three-phase equilibria proven by experimental data are marked with an asterisk. The Ce-solubility in (Mg), which is only 8×10^{-8} at.% Ce in the binary Mg–Ce, is further reduced by addition of Zn to 0.02×10^{-8} at.% Ce at the three-phase point (Mg) + $CeMg_{12}$ + T2. This edge is at 1.3 at.% Zn (3.4 wt.% Zn), which means that (Mg) with less Zn is saturated with $CeMg_{12}$ while beyond that (Mg) + T2 prevails up to the limit of 2.4 at.% Zn in (Mg) at the (Mg) + T2 + MgZn equilibrium.

The phase diagram section calculated at constant 85 at.% Mg, including the DSC signals from samples #1–#3, is shown in Fig. 3. The strong heating and cooling signal shown by sample #1 at the invariant reaction U8 is most decisive. Also the liquidus temperatures of samples #1 and #2 are well reproduced by the calculation while the liquidus temperature of sample #3, calculated at 639 °C, could not be detected.

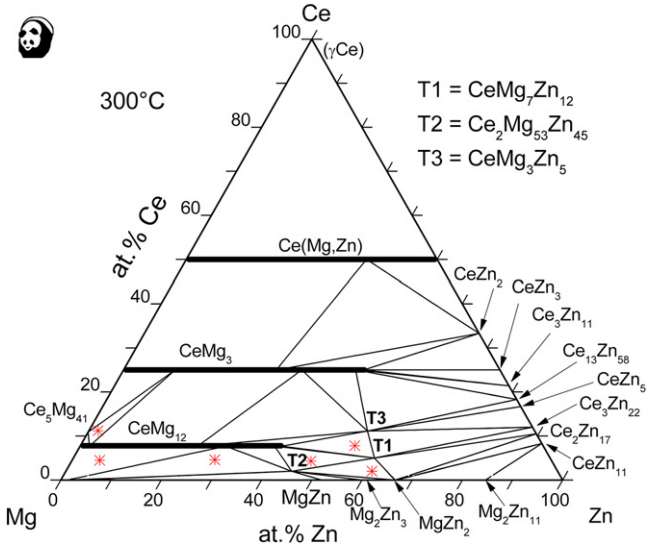

Fig. 2. Calculated isothermal section at 300 °C. Tie-triangles marked with * are validated by experimental data.

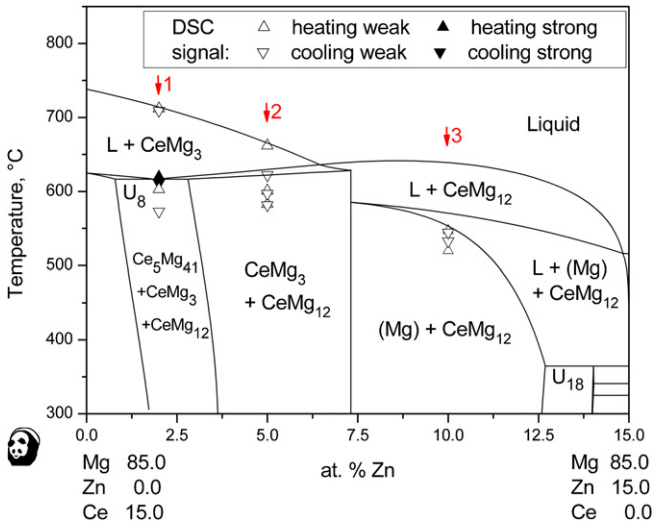

Fig. 3. Calculated vertical phase diagram section at constant 85 at.% Mg including the DSC signals from samples #1–#3.

5.3. Solidification paths and microstructures of Mg-rich alloys

Microstructures of the samples in the Mg-rich corner were investigated in detail. Samples #1–#3 in fact exhibit the phase sequence and primary crystallizing phases given by the calculation in Fig. 3. The back-scattered electron micrograph (BSE) of sample #1 (Ce13–Mg85–Zn2) solidified at 5 K min^{-1} is shown in Fig. 4. Primary crystallized dendrites of $CeMg_3$ (with 3 at.% Zn-solubility) are enlaced by secondary $CeMg_{12}$ and some Ce_5Mg_{41}. This microstructure is confirmed by the calculated invariant reaction U8: $L + CeMg_3 \rightarrow CeMg_{12} + Ce_5Mg_{41}$ at 617 °C; the calculated phase amounts reveal that this is almost a eutectic reaction ($L \rightarrow CeMg_{12} + Ce_5Mg_{41}$) with only a negligible amount of $CeMg_3$ being consumed. This finding is further corroborated by the strong thermal signals detected at that temperature by DSC in the same sample, see Table 2 and Fig. 3.

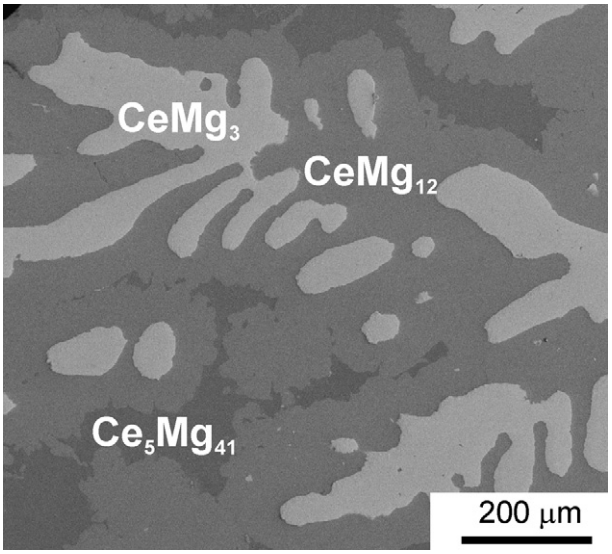

Fig. 4. Electron micrograph (BSE) of sample #1 (Ce13–Mg85–Zn2) solidified at 5 K min^{-1}, showing the primary dendrites of $CeMg_3$ (bright, with 3 at.% Zn), secondary $CeMg_{12}$ (middle gray) and some Ce_5Mg_{41} (slightly darker) both formed in the calculated invariant reaction U8, also detected by DSC in this sample.

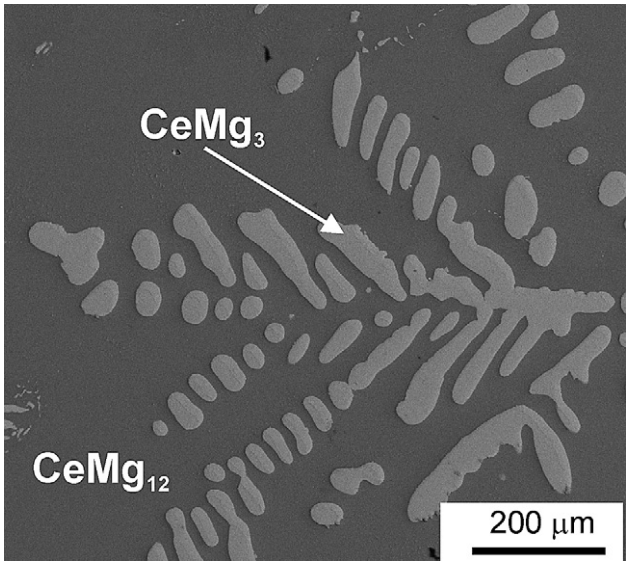

Fig. 5. Electron micrograph (BSE) of sample #2 (Ce10–Mg85–Zn5) solidified at 5 K min^{-1}, showing the primary dendrites of $CeMg_3$ (bright, with 9 at.% Zn) together with secondary $CeMg_{12}$ as predicted by thermodynamic calculation.

In sample #2 (Ce10–Mg85–Zn5) the microstructure in Fig. 5 reveals again primary dendrites of $CeMg_3$ (with 9 at.% Zn-solubility) with subsequent crystallization of $CeMg_{12}$ (with 3 at.% Zn-solubility). This is entirely consistent with the calculated two-phase equilibrium solidus structure of this sample.

The phase diagram section, Fig. 3, indicates that the primary phase changes from $CeMg_3$ to $CeMg_{12}$ beyond 6.5 at.% Zn. Indeed, sample #3 (Ce5–Mg85–Zn10) shows primary crystallization of the phase $CeMg_{12}$ (with 15 at.% Zn-solubility) in Fig. 6. The secondary phase is (Mg) with 1 at.% Zn dissolved and no measurable content of Ce, using SEM/EDS.

Finally the electron micrograph (BSE) of sample #5 (Ce42–Mg56–Zn2) in Fig. 7 shows the primary dendrites of $CeMg_2$ (with 1 at.% Zn-solubility) with secondary Ce(Mg,Zn). The calculation

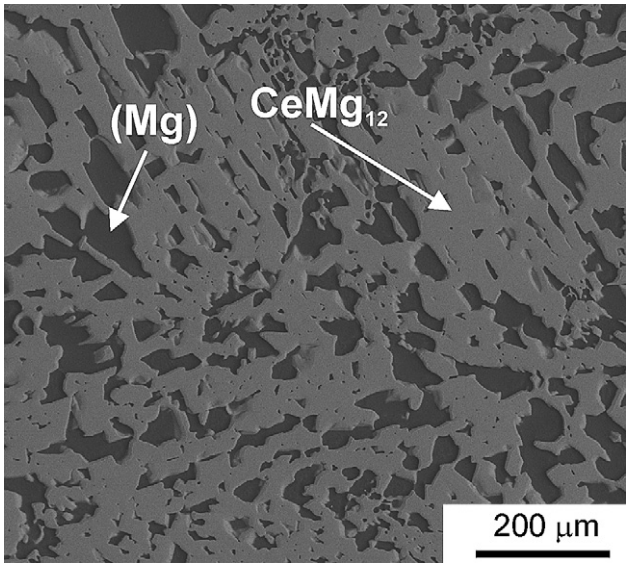

Fig. 6. Electron micrograph (BSE) of sample #3 (Ce5–Mg85–Zn10) solidified at 5 K min^{-1}, showing the primary $CeMg_{12}$ (bright, with 15 at.% Zn) together with secondary (Mg) as predicted by thermodynamic calculation.

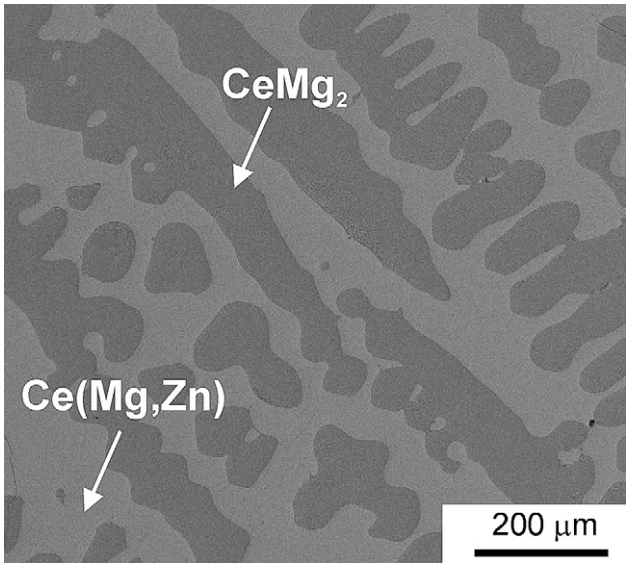

Fig. 7. Electron micrograph (BSE) of sample #5 (Ce42–Mg56–Zn2) solidified at 5 K min^{-1}, showing the primary dendrites of $CeMg_2$ (dark, with 1 at.% Zn) together with secondary Ce(Mg,Zn) as predicted by thermodynamic calculation.

reveals that this solidification $L \rightarrow CeMg_2 + Ce(Mg,Zn)$ occurs in the narrow temperature range of 730–721 °C, thus generating strong thermal liquidus signals. This sample runs very close to the invariant reaction U1, $L + CeMg_3 \rightarrow Ce(Mg,Zn) + CeMg_2$ at 729 °C which could be met if the sample had lost some Ce.

6. Conclusion

On the experimental side our work focuses on the Mg-rich part of the ternary system. Sample compositions were chosen from 34 to 85 at.% Mg from preliminary calculations indicating these to be most decisive for determination of thermodynamic parameters and verification of invariant liquidus reactions and solid state equilibria up to pure magnesium. The final thermodynamic modeling, however, covers the entire range of the Mg–Zn–Ce system. The Zn–Ce-rich region of the Mg–Zn–Ce system is calculated based on the extrapolation from the thermodynamic descriptions of the edge binary phases. Additional experimental data particularly in the Zn-rich corner are required to establish the phase equilibria of this ternary system completely.

All solid solubilities of Zn in Mg–Ce intermetallic phases are due to substitutional exchange of Mg by Zn. The large Zn-solubilities of the $CeMg_{12}$ and $CeMg_3$ phases are treated as two single phases ($CeMg_{12}$ up to 40 at.% Zn and $CeMg_3$ up to 48 at.% Zn at 300 °C). This might be considered as simplification since [6] described different crystal structures and two-phase field between these phases. However, these observations could not be confirmed by Ref. [12] and in this work.

It is remarkable that extremely small solubilities of Ce in Mg–Zn liquid alloys are observed beyond which Ce-containing intermetallic phases precipitate, namely $CeMg_{12}$, $Ce_2Mg_{53}Zn_{45}$ (T2), and $CeMg_7Zn_{12}$ (T1). The (Mg) phase crystallizes jointly only with $CeMg_{12}$ and T2, the transition between these two secondary phases occurs at the invariant reaction U15 at 420 °C with a liquid composition of Mg76.6–Zn23.4–Ce0.003 (at.%). The transition in the solid state equilibria of (Mg) at 300 °C occurs at 1.3 at.% Zn (3.4 wt.% Zn), which means that (Mg) with less Zn is saturated with $CeMg_{12}$; in the (Mg) solid solution from 1.3 to 2.4 at.% Zn the secondary phase is T2.

Termination of ternary solidification involving (Mg) and secondary phases under equilibrium conditions is given by the reaction $L + (Mg) \rightarrow Mg_7Zn_3 + T2$ (U19) at 341.02 °C. If this transition-type reaction does not go to completion, the final ternary eutectic, $L \rightarrow MgZn + Mg_7Zn_3 + T2$ (E4) at 340.99 °C may be reached. Both invariant reactions are calculated at negligible composition of Ce in the liquid ($<10^{-5}$ at.% Ce), and consequently only a negligible amount of T2 forms and the temperatures are virtually identical (within less than 0.01 K) to those of the corresponding binary Mg–Zn reactions. Therefore, the ternary eutectic temperature reported by Ref. [5] at 342 ± 1 °C may be interpreted only as verification that the invariant reaction E4 calculated at 341 °C is indeed very close to the binary one. On the same grounds the calculated liquid composition of E4 (29.0 at.% Zn) is virtually identical to the adjunct binary one. The difference to the reported composition of 25.9 at.% Zn, given by Ref. [5], cannot be due to a shift of the eutectic trough in the ternary. It is probably caused by the experimental uncertainty related to the binary value that is calculated here from the latest thermodynamic assessment of the Mg–Zn system [11].

Acknowledgements

This study is supported by the German Research Foundation (DFG) in the Priority Programme "DFG-SPP 1168: InnoMagTec" under grant no. Schm 588/27.29.

References

[1] Bamberger M. Structural refinement of cast magnesium alloys. Mater Sci Technol 2001;17:15–24.
[2] Zhu YM, Morton AJ, Nie JF. Improvement in the age-hardening response of Mg–Y–Zn alloys by Ag additions. Scripta Mater 2008;58:525–8.
[3] Nie JF, Oh-ishi K, Gao X, Hono K. Solute segregation and precipitation in a creep- resistant Mg–Gd–Zn alloy. Acta Mater 2008;56:6061–76.
[4] Chino Y, Sassa K, Mabuchi M. Tensile properties and stretch formability of Mg–1.5 mass% Zn–0.2 mass% Ce sheet rolled at 723 K. Mater Trans 2008;49:1710–2.
[5] Korol'kov AM, Sal'dau YaP. Solubility of Zn and Ce in Mg in the solid state. Izv Sekt Fiz-Khim Anal 1946;16:295–306 (in Russian).
[6] Mel'nik EV, Kostina MF, Yarmolyuk YaP, Zmii OF. Study of magnesium–zinc–cerium and magnesium–zinc–calcium ternary systems, in: Mater. Vses. Soveshch. Issled., Razrab. Primen. Magnievyhk Splavov 1978:95–9.
[7] Kolitsch U, Bellen P, Kaesche S, Macciò D, Bochvar N, Liberov Y, et al. Cerium–magnesium–zinc. In: Petzow G, Effenberg G, editors. Ternary alloys: a comprehensive compendium of evaluated constitutional data and phase diagrams, vol. 17. Stuttgart, Germany: Weinheim: VCH Verlagsgesellschaft, MSI GmbH; 2000. p. 168–76.
[8] Drits ME, Drozdova EI, Korol'kova IG, Kinzhibalo VV, Tyvanchuk AT. Investigation of polythermal sections of the Mg–Zn–Ce system in the Mg-rich region. Russ Metall 1989;2:195–7.
[9] Mel'nik EV, Zmii OF, Cherkasim EE. On the structure of the $Ce_2Mg_3Zn_3$ compound. Vestn L'viv Univ Ser Khim 1977;19:34–6 (in Russian).
[10] Cacciamani G, Borzone G, Ferro R. System Ce–Mg. European Commission EUR 18499 EN. In: Ansara I, Dinsdale AT, Rand MH, editors. COST 507—thermochemical database for light metal alloys, July 1998; 1998. p. 137–40.
[11] Agarwal R, Fries SG, Lukas HL, Petzow G, Sommer F, Chart TG, et al. Assessment of the Mg–Zn system. Z Metallkd 1992;83:216–23.
[12] Kevorkov D, Pekguleryuz M. Experimental study of the Ce–Mg–Zn phase diagram at 350 °C via diffusion couple techniques. J Alloys Compd 2009;478:427–36.
[13] Sato TJ, Abe E, Tsai AP. Composition and stability of decagonal quasicrysatls in the Zn–Mg-rare-earth systems. Phil Mag Lett 1998;77:213–9.
[14] Pavlyuk V, Solokha P, Dmytriv G, Marciniak B, Paul-Boncour V. The Heusler-type alloy $MgZn_2Ce$. Acta Crystallogr Sect. E Struct Rep Online E63 2007:i161.
[15] Pavlyuk V, Solokha P, Zelinska O, Paul-Boncour V, Nowik-Zajac A. Ce20Mg19Zn81: a new structure type with a giant cubic cell. Acta Crystallogr Sect C Cryst Struct Comm 2008;C64:i50–2.
[16] Wang CP, Chen X, Liu XJ, Pan FS, Ishida K. Thermodynamic modeling of the Ce–Zn and Pr–Zn systems. J Alloys Compd 2008;458:166–73.
[17] Dinsdale AT. SGTE data for pure elements. Calphad 1991;15:317–425.
[18] Redlich O, Kister AT. Thermodynamics of nonelectrolytic solutions. Algebraic representation of thermodynamic properties and the classification of solutions. Ind Eng Chem 1948;40:345–8.
[19] Hillert M. The compound energy formalism. J Alloys Compd 2001;320:161–76.
[20] Chen SL, Daniel S, Zhang F, Chang YA, Yan XY, Xie FY, et al. The PANDAT software package and its applications. Calphad 2002;26:175–88.